Relationship between sea level and climate forcing by CO_2 on geological timescales

Gavin L. Foster[a,1] and Eelco J. Rohling[a,b]

[a]Ocean and Earth Science, National Oceanography Centre Southampton, University of Southampton Waterfront Campus, Southampton SO14 3ZH, United Kingdom; and [b]Research School of Earth Sciences, Australian National University, Canberra, ACT 0200, Australia

Edited by Mark H. Thiemens, University of California at San Diego, La Jolla, CA, and approved November 28, 2012 (received for review September 18, 2012)

On 10^3- to 10^6-year timescales, global sea level is determined largely by the volume of ice stored on land, which in turn largely reflects the thermal state of the Earth system. Here we use observations from five well-studied time slices covering the last 40 My to identify a well-defined and clearly sigmoidal relationship between atmospheric CO_2 and sea level on geological (near-equilibrium) timescales. This strongly supports the dominant role of CO_2 in determining Earth's climate on these timescales and suggests that other variables that influence long-term global climate (e.g., topography, ocean circulation) play a secondary role. The relationship between CO_2 and sea level we describe portrays the "likely" (68% probability) long-term sea-level response after Earth system adjustment over many centuries. Because it appears largely independent of other boundary condition changes, it also may provide useful long-range predictions of future sea level. For instance, with CO_2 stabilized at 400–450 ppm (as required for the frequently quoted "acceptable warming" of 2 °C), or even at AD 2011 levels of 392 ppm, we infer a likely (68% confidence) long-term sea-level rise of more than 9 m above the present. Therefore, our results imply that to avoid significantly elevated sea level in the long term, atmospheric CO_2 should be reduced to levels similar to those of preindustrial times.

Sea-level change is one of the most significant and long-lasting consequences of anthropogenic climate change (1). However, accurate forecasting of the future magnitude of sea-level change is difficult because current numerical climate models lack the capacity to accurately resolve the dynamical processes that govern size changes of continental ice sheets [e.g., total disappearance of the current continental ice sheets would raise mean sea level by about 70 m (1)]. This complicates long-range sea-level projections because the retreat of continental ice sheets will increasingly contribute to sea-level rise as the 21st century progresses (2), and because this rise will continue long into the future, even if temperatures were stabilized, according to different mitigation scenarios for greenhouse gas emissions (1). Because of the absence of adequate ice-dynamical processes in models, even the most recent estimates have to rely on assumed (linear) relationships between ice-volume reduction and global mean temperature increase (1), which as yet remain largely untested. Therefore, here we provide a natural context to projections of future long-term (multicentury) sea-level rise, by assessing key relationships in the Earth's climate system using recent high-quality data from the geological past. Because global mean temperature is hard to measure in the geological past without applying (often problematic) assumptions about polar amplification or deep-sea temperature relationships (3, 4), we instead concentrate on quantifying the "likely" [68% probability (5)] long-term relationship between two entities that can be measured more directly, namely ice-volume/sea-level and CO_2 levels.

Data from gas bubbles in ice-core samples provide a high-fidelity CO_2 record for the last 800,000 y (6–8) that, when coupled with sea-level records of similar resolution (9), illustrates that CO_2 and sea level are intimately related on these timescales (Fig. 1). This relationship arises because CO_2 is the principal greenhouse gas that amplifies orbital forcing and to a large extent determines the thermal state of the Earth system across glacial–interglacial cycles and thus the amount of ice stored on land (3). In detail, there are short leads and lags between Earth system components because of different timescales of inertia, but the overall relationship is strong ($R^2 = 0.68$; $n = 2051$; Fig. 1).

Radiative forcing of climate by CO_2 changes is logarithmic in nature (10), and the relationship between $\ln(CO_2/C_0)$ (where C_0 = 278 ppm = preindustrial CO_2) and sea level over the past 550,000 y can be well approximated by a linear fit (Fig. 1*B*). However, this linear relationship cannot be simply extended beyond the data—for instance, to predict changes for increasing CO_2 forcing—because the sea-level response to CO_2 forcing below 280 ppm relates to the growth and retreat of large ice sheets that extended to relatively low latitudes in the Northern Hemisphere, and which today no longer exist [the Laurentide and Fennoscandian ice sheets (11)]. Sea-level change in the future instead will be dominated by changes in the ice sheets that have remained, mostly at higher latitudes: the Greenland Ice Sheet (GrIS), Western Antarctic Ice Sheet (WAIS), and Eastern Antarctic Ice Sheet (EAIS). The threshold CO_2 required for the retreat of these ice sheets is clearly higher than the preindustrial level of 280 ppm; otherwise, they would have been in retreat during the current interglacial before the anthropogenic CO_2 increase [sea-level data show that ice volume has been stable for at least the last 3,000–5,000 years (12)]. To assess the equilibrium response of these ice sheets to CO_2 forcing, we must examine the geological record well beyond 550,000 y ago, to include times when the Earth's climate was significantly warmer than today. The Cenozoic Era (0–65 Ma) contains several time periods when the Earth was warmer, CO_2 was higher, and continental ice volume was reduced, relative to the present. Here, we compile reconstructions of atmospheric CO_2 concentrations and sea level from a variety of proxies and archives (ice cores and sediment cores) from the last 40 My, to better determine the nature of the relationship between these two variables on geological timescales.

Our atmospheric CO_2 data, displayed as a number of time series in Fig. 2, come from three methods: (*i*) gas bubbles trapped in ice cores [0–550 kya (6–8)]; (*ii*) the carbon isotopic composition of sedimentary alkenones recovered from deep-sea sediments—the fractionation between alkenones and total dissolved carbon in seawater is largely a function of $[CO_2]_{aq}$ [20–38 Ma (13)]; and (*iii*) the boron isotopic composition of planktic foraminifera from deep-sea sediments, which depends on pH (e.g., ref. 14), from which $[CO_2]_{aq}$ and atmospheric CO_2 can be calculated [2.7–3.2 Ma, 11–17 Ma, and 33–36 Ma (15–18)]. Those methods, based on deep ocean sediments, can reproduce the ice-core CO_2 record accurately (19–22), but each has several inherent uncertainties. However, over

EARTH, ATMOSPHERIC, AND PLANETARY SCIENCES

Author contributions: G.L.F. and E.J.R. designed research, performed research, analyzed data, and wrote the paper.

The authors declare no conflict of interest.

This article is a PNAS Direct Submission.

[1]To whom correspondence should be addressed. E-mail: gavin.foster@noc.soton.ac.uk.

This article contains supporting information online at www.pnas.org/lookup/suppl/doi:10.1073/pnas.1216073110/-/DCSupplemental.

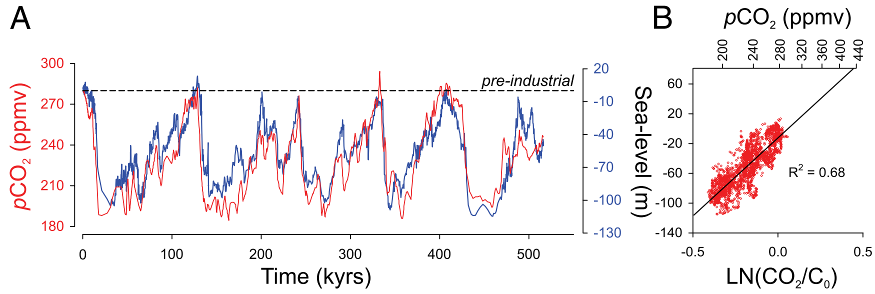

Fig. 1. The relationship between the partial pressure of atmospheric CO_2 (ppmv) and global sea level (m). (*A*) The record of CO_2 and sea level over the past 550,000 y (6–9). The dotted horizontal line denotes preindustrial values for each variable. (*B*) Cross-plot of pCO_2 [and $\ln(CO_2/C_0)$] against sea level (m) for the same data shown in *A*. A linear best-fit line is shown with an R^2 (correlation coefficient) = 0.68.

recent years there has been a trend toward increasing agreement between pre–ice-core CO_2 estimates (23), and for our chosen time intervals, there is, on the whole, a good agreement among the δ^{11}B-based, δ^{13}C-based, and stomatal index-based estimates (Fig. S1). The notable exception is the Miocene (11–17 Ma) time slice, in which in parts, only stomatal and δ^{11}B-based estimates agree (see discussion in *SI CO2 and Sea-Level Estimates* and ref. 18). Nonetheless, overall agreement among multiple proxies provides confidence in the higher-resolution marine-based records we have chosen to use here.

The sea-level records we use also derive from several methods and sources, and also are displayed in time series in Figs. 1 and 2: (*i*) changes in the oxygen isotopic composition of foraminifera and bulk carbonate from Red Sea sediments, which predominantly record sea level [Pleistocene, 0–550 kya (24–25)]; (*ii*) backstripping of marginal sediments combined with estimates of paleowater depth based on detailed lithofacies, ichnological, and benthic foraminiferal analyses [Pliocene (2.7–3.2 Ma) and Eocene–Oligocene (20–38 Ma) (26, 27)]; and (*iii*) sea-level change reconstructed using Mg/Ca of foraminifera to isolate the ice-volume signal from foraminiferal δ^{18}O. Because of uncertainties in the Mg/Ca of seawater (see ref. 27 and references therein), we calculate only relative sea-level records using this approach and pin them to either a highstand from backstripping [Miocene (11–17 Ma) (28)] or an estimate of an ice-free world [+64 m; Eocene–Oligocene (33–36 Ma)]. Other sea-level records are available for these time periods, and there generally is a good agreement among different methodologies for the same time period, which provides a high degree of confidence in the reconstructions (Fig S2 and ref. 26). Again, a notable exception is the Miocene (11–17 Ma), when sea level from backstripping from the New Jersey margin (NJM) is particularly problematic (29). However, the record we use here, based on δ^{18}O (*SI CO2 and Sea-Level Estimates*), agrees well with backstripping from the Marion Plateau, Australia (29). We have been conservative in our assignment of uncertainty for all data used; beyond 550 kya, typical uncertainty at 95% confidence is ±15–30% for CO_2 and ±25–30 m for sea level. More extensive details about these methods and the approaches we have followed may be found in *SI CO2 and Sea-Level Estimates*.

The compiled CO_2 and sea-level records cover about two thirds of the last 40 My, but not in a continuous fashion (Fig. 2), and we restrict our selection to the time periods with the highest density of data for both sea-level and CO_2. Although other variables and boundary conditions that influence ice growth/retreat also may have changed between the time intervals (e.g., ocean gateway configurations, continental positions, and orography), we focus here on establishing the first-order relationships and accept that these may be refined further by future studies.

Results and Discussion

A combination of data from all five time slices (Fig. 3*A*) reveals that on these longer timescales, there is a clearly sigmoidal relationship between sea level and climate forcing by CO_2. Moreover, there is a striking similarity between data from different time periods and those generated by different techniques (e.g., Fig. 3*A*). This overall agreement implies that this relationship is robust and reflects the fundamental behavior of the Cenozoic climate system, despite some significant changes in boundary conditions (e.g., closing of the Panama Gateway since the Pliocene, closure of Tethys since the Miocene). In detail, it is evident that for CO_2 between ~200 and ~300 ppm (data from the Pleistocene, Pliocene, and Miocene), the relationship is similar to that defined by the ice-core data alone (Fig. 1), whereas the sea-level estimates remain rather "flat" within the range −10 ± 10 to +20 ± 10 m (68% confidence, see below) for CO_2 values between ~400 and ~650 ppm (Fig. 3*A*; defined by data from the Pliocene, Miocene, and Oligocene). At CO_2 > 650 ppm, CO_2 changes again are associated with sustained changes in sea level (Fig. 3*A*; defined by data from the Eocene and Oligocene).

Because of the nature of Cenozoic climate change, many of the data points derive from periods of global cooling and declining CO_2 (30). However, for the Miocene, Pleistocene, and Eocene–Oligocene, there also are data from warming intervals in which CO_2 is increasing (Figs. 1 and 2). In the Pleistocene (CO_2 < 280 ppm), there is no evidence of hysteresis beyond a few thousand years; intervals with increasing and decreasing CO_2 give a similar sea-level response (Fig. 1), as also was elaborated for the relationship between sea level and temperature in that period (9). Similarly, for the Miocene (CO_2 < 450 ppm), there is no evidence of hysteresis within a temporal resolution of ~300,000 y (Fig. 2). Conversely, the Eocene–Oligocene data show some suggestion of hysteresis (*SI CO2 and Sea-Level Estimates* and Fig. S3). As yet, this remains insufficiently defined, but it concerns only times with CO_2 > 800 ppm (Fig. S3).

To facilitate a quantitative comparison between $\ln(CO_2/C_0)$ and sea level, we have performed a probabilistic analysis. For this analysis, we randomly perturbed all data points within normal distributions characterized by their mean and SDs (recalculated so as to be symmetrical), then applied a statistical B-spline smoothing fit with automated node detection. This procedure was repeated 300 times, followed by an assessment of the distributions of sea-level values per CO_2 step, where we determined the probability maximum (distribution peak) as well as the 68% and 95% probability intervals (using the 16% and 84% percentiles, and the 2.5% and 97.5% percentiles). Removal of any one particular dataset does not result in a significantly different geometry to the distribution of the probability maximum. This assessment (Fig. 3*B*) clearly reveals a sea-level "plateau" at around 22 m between CO_2 levels of about 400 and 650 ppm, with average 68% confidence limits for this interval of $^{+13}/_{-12}$ m, which covers sea-level values

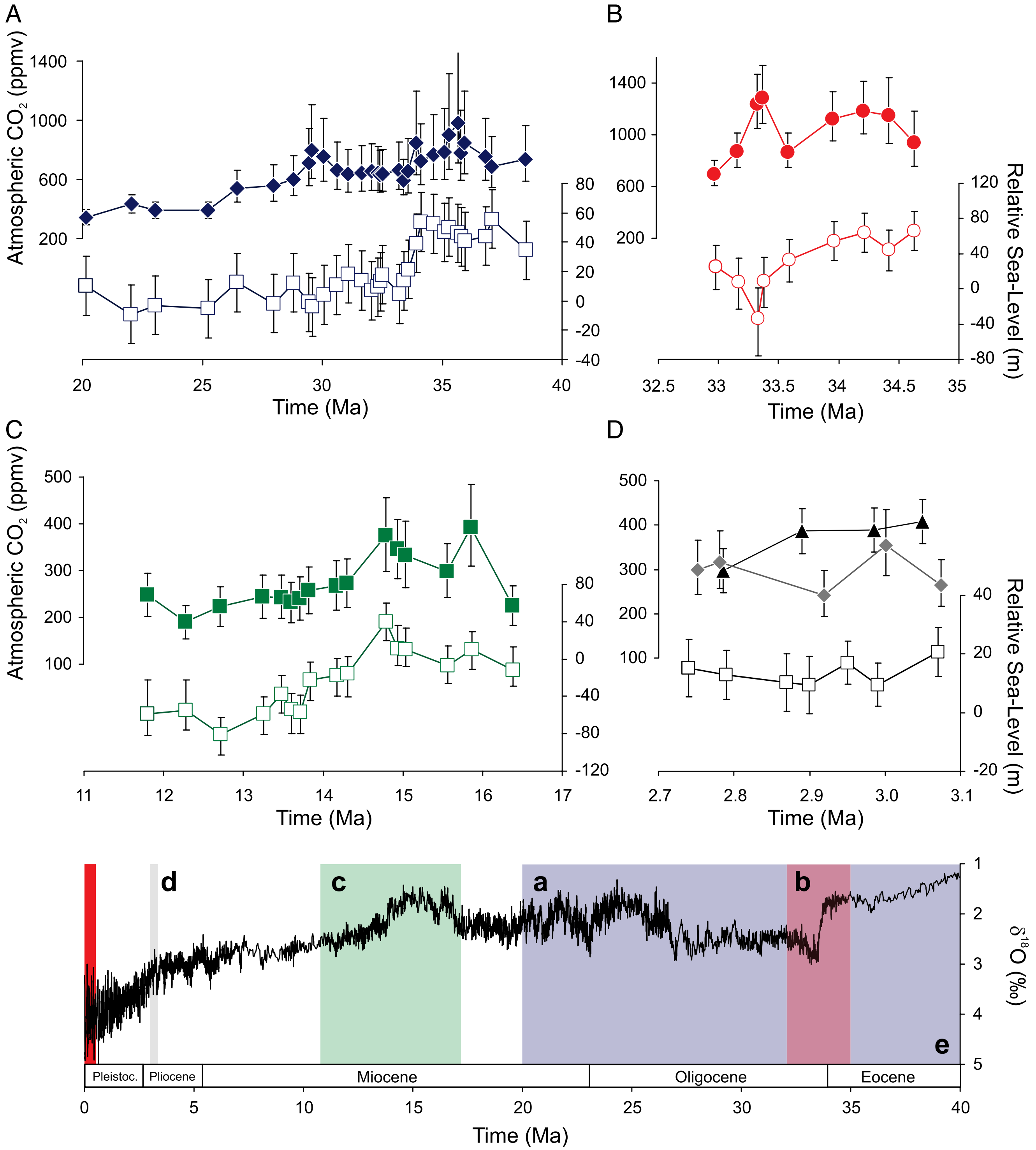

Fig. 2. Time series of sea-level and CO_2 data used to construct Fig. 3. (*A*) Alkenone $\delta^{13}C$ based CO_2 (13) and sea level based on sequence stratigraphy of the NJM (27). (*B*) Boron isotope-based CO_2 record (15) with sea level based on the oxygen isotope composition of planktic foraminifera fixed at ice-free (e.g., pre-Eocene–Oligocene boundary) = + 65 m (*SI CO2 and Sea-Level Estimates*). (*C*) Boron isotope-based CO_2 record (18) with sea level from the benthic foraminiferal $\delta^{18}O$ (45) fixed to the Miocene highstand of the NJM sequence stratigraphic record (28) (*SI CO2 and Sea-Level Estimates*). (*D*) Boron isotope-based CO_2 records (gray diamonds) (17) and (black triangles) (16). Sea-level record from a compilation (26) using several methodologies, including sequence stratigraphy and benthic foraminiferal $\delta^{18}O$ corrected for temperature (see ref. 26 for details). Note CO_2 and highstands do not correlate exactly in time, but in each case sea-level estimate and CO_2 are within 10,000 y. (*E*) Benthic oxygen isotope stack (30) with the locations of the time slices shown in *A*–*D* (and Fig. 1), shown as appropriately colored and labeled band. All data displayed in (*A*–*D*) can be found in Dataset S1.

that might be expected in the absence of GrIS and WAIS [+14 m (31)], although within the bounds of uncertainty, we cannot rule out that there was an additional component of mass reduction in the EAIS at these midlevel CO_2 values (18, 32). Based on the probability maximum and full contributions from GrIS and WAIS, this may have been equivalent to about 10 m of sea-level rise.

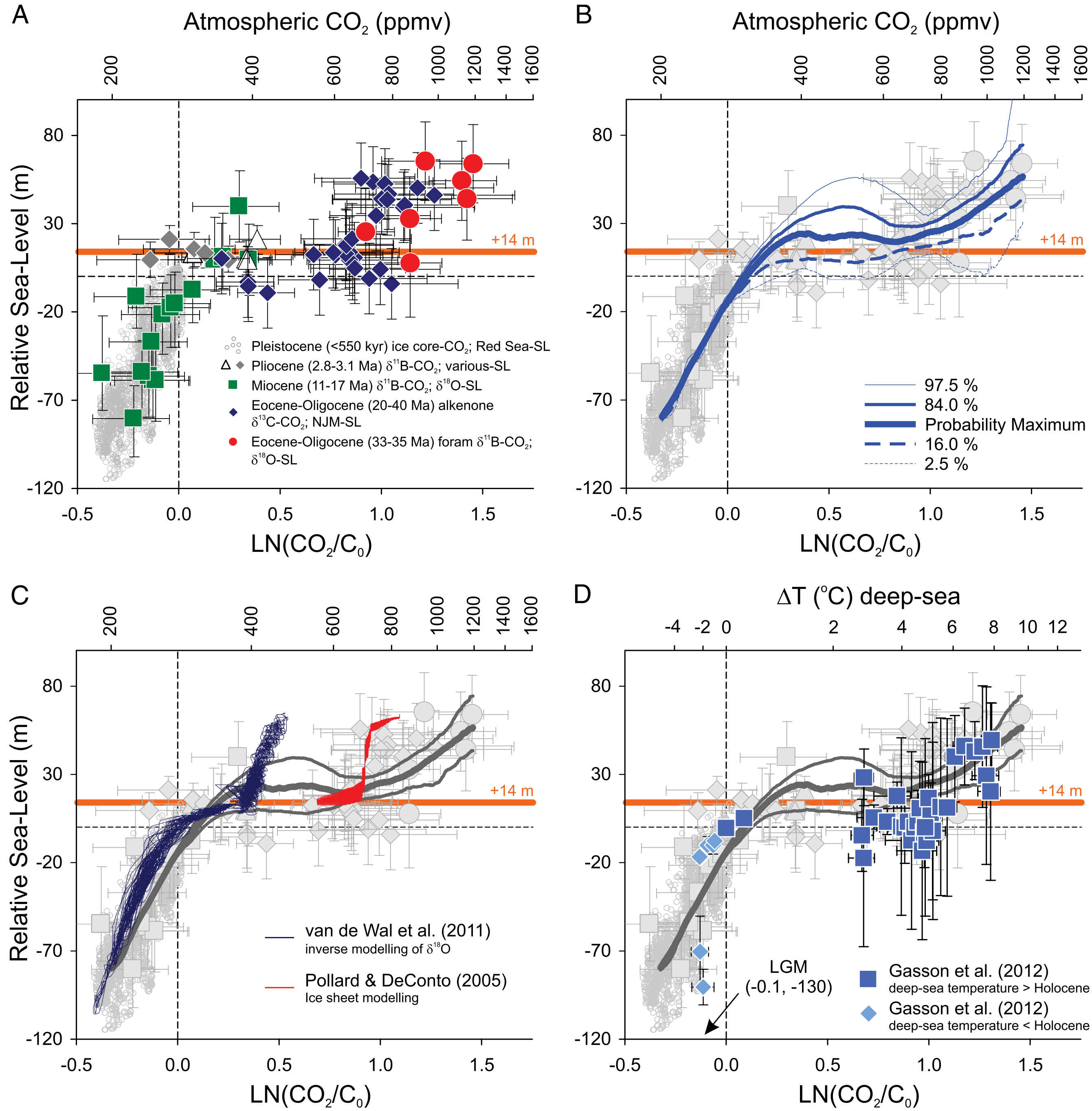

Fig. 3. Cross-plot of estimates of atmospheric CO_2 and coinciding sea level. (*A*) Data are split according to time period and technique used. Symbols as in Fig. 2. Note for the Eocene–Oligocene from $\delta^{11}B$ and $\delta^{18}O$, only data that form a decreasing CO_2 trend are plotted for clarity. (*B*) Results from our probabilistic analysis of the data that fully accounts for uncertainty in both X and Y parameters (see text; Dataset S2). (*C*) Data shown in Fig. 3*A* along with EAIS ice-sheet model output (37) for declining CO_2 with orbital variation (red) and the results of inverse modeling of $\delta^{18}O$ (blue) (39). (*D*) Relative deep-sea temperature change (ΔDST; second *x*-axis) and sea-level compilation (blue) (40). ΔDST has been scaled by assuming (*i*) for ΔDST > 0, ΔDST = global temperature change (ΔT_{global}), when ΔDST < 0, ΔDST = $\Delta T_{global}/1.5$ (following ref. 46); and (*ii*) for a ΔDST > 0 climate sensitivity of 2.96 K per CO_2 doubling (4), for a ΔDST < 0 a climate sensitivity of 11.5 K per CO_2 doubling (4). The last glacial maximum (LGM) datapoint from ref. 40 lies outside this plot at -0.1 ± 0.1, -130 ± 10 m (indicated by arrow). On all panels, dotted lines denote the preindustrial conditions of 0 m and 280 ppm CO_2. The horizontal orange line shows +14 m, which is the sea-level rise associated with the total melting of WAIS and GrIS (31). For *C* and *D*, the least-squares spline fit through the data (thick gray lines) is shown only as a probability maximum and 84 and 16 percentiles for clarity.

Our observed long-term relationship between sea level and CO_2 forcing reaffirms the importance of CO_2 as a main driver of changes in the Earth's climate over the past 40 My. The exact nature of the relationship can be understood in the context of the ice sheets involved. During the Eocene, when CO_2 levels were higher than 1,000 ppm, sea level was 60–70 m higher than today, reflecting the absence of any of the major ice sheets that currently reside at high latitudes (30). Sea-level change during the Eocene–Oligocene, with CO_2 in general decline from 1,000 ppm to 650 ppm (13, 15), was driven largely by buildup of the EAIS

(33). Our $\ln(CO_2/C_0)$–sea-level (SL) [$\ln(CO_2/C_0)$:SL] relationship indeed suggests there was strong ice-sheet (EAIS) expansion with CO_2 decline during those times (Fig. 3*A*). Next, we observe a lack of long-term sea-level response for CO_2 levels between about 650 and 400 ppm. This suggests that during these times, very little continental ice grew (or retreated); presumably CO_2 was too high, hence the climate too warm to grow more continental ice after the "carrying capacity" of the EAIS had been reached (Fig. 3*A*). It also suggests that 300–400 ppm is the approximate threshold CO_2 value for retreat and growth, respectively, of WAIS and GrIS (and possibly a more mobile portion of EAIS). Sea levels of 20–30 m above the present during the Pliocene and Miocene, when CO_2 was largely between 400 and 280 ppm, are thought to predominantly reflect mass changes in the GrIS and WAIS (26, 31). However, recent records proximal to the Antarctic ice sheet indicate that some portion [maybe as much as 10 m sea-level equivalent (26, 34)] of the EAIS also retreated during these warm periods (26, 35). Finally, sea levels lower than those of the present, as observed during the last 550,000 y and during the Miocene, were caused largely by growth of the Laurentide and Fennoscandian ice sheets (11, 18). As also argued before, the threshold CO_2 value for the growth of these ice sheets must be below 280 ppm (6); a recent assessment suggests that with our current orbital configuration, a threshold of 240 ± 5 ppm is appropriate (36).

This study directly determines the relationship between CO_2 and sea level from data covering the entire range of climates experienced by the Earth over the past 40 My. We find a strong similarity to nonlinear relationships that have been proposed by ice-sheet modeling (37, 38), theoretical studies (39), and a recent synthesis of deep-sea temperature and sea level for the past 10–40 My (40). A comparison between our work and these earlier studies is shown in Fig. 3 *C* and *D*. Our data compilation and probabilistic analysis are in good agreement with the deep-sea temperature:sea-level compilation (40) (Fig. 3*D*) and ice-sheet modeling output (37) (Fig. 3*C*). However, although the overall shape of our $\ln(CO_2/C_0)$:SL relationship is similar to that inferred using inverse modeling of the benthic foraminiferal $\delta^{18}O$ record (39), our compilation places the transition from a nonglaciated to fully glaciated EAIS at considerably higher CO_2 (650–1,000 ppm CO_2 vs. their 380–480 ppm CO_2; Fig. 3*C*).

Our quantitative $\ln(CO_2/C_0)$:SL relationship reflects the long-term (greater than orbital timescales) near-equilibrium relationship between these variables. Because it is constrained by real-world observations of the Earth system, our relationship inherently includes all feedbacks and processes that contribute to sea-level change. It also appears to be largely independent of other boundary condition changes and therefore may be used with confidence to determine a likely estimate for sea level if the Earth system were to reach equilibrium with modern or future CO_2 forcing. Given the present-day (AD 2011) atmospheric CO_2 concentration of 392 ppm, we estimate that the long-term sea level will reach $+24\,^{+7}/_{-15}$ m (at 68% confidence) relative to the present. This estimate is an order of magnitude larger than current projections for the end of this century [up to 2 m; best estimate, 0.8 m (41)] and seems closer to the worst-case long-term sea-level projection portrayed by Meehl et al. (1). Using terminology of the Intergovernmental Panel on Climate Change Fourth Assessment Report IPCC AR4 (5), we find it very likely (i.e., at 90% confidence) that long-term sea-level rise for sustained present-day CO_2 forcing will be >6 m, and likely (68% confidence) that it will be >9 m. Through analogy with the geological record, this rise likely will be achieved through melting of the GrIS and WAIS and possibly some portion of the EAIS (if sea level were to rise >14 m). However, it will take many centuries to get to these high levels. Given the typical mean rates of natural sea-level rises on multicentury timescales [1.0–1.5 $cm \cdot yr^{-1}$, with extremes during deglaciation of 5 $cm \cdot yr^{-1}$ (41–43)], our projection suggests an expected equilibration time of the Earth system to modern CO_2 forcing of 5–25 centuries. Notably, however, this is likely still faster than the rates at which CO_2 is removed from the atmosphere via natural processes (deep-sea sediment dissolution and silicate weathering), which operate on 10,000–100,000-y timescales (44).

Clearly our relationship has limited relevance to short-term sea-level projections for the next century. However, accurately determining the long-term response of sea level to CO_2 forcing has significant implications for the long-term stabilization of greenhouse gas emissions (by natural processes or human activity) and for decisions about the "acceptable" long-term level of CO_2/warming. For instance, our results imply that acceptance of a long-term 2 °C warming [CO_2 between 400 and 450 ppm (46)] would mean acceptance of likely (68% confidence) long-term sea-level rise by more than 9 m above the present. Future studies may improve this estimate, notably by better populating the interval between CO_2 concentrations of 500–280 ppm (i.e., the Pliocene/middle Miocene). Regardless, the current relationship is sufficiently refined to imply that CO_2 would need to be reduced significantly toward 280 ppm before any lost ice volume might be regrown (similarly over many centuries).

ACKNOWLEDGMENTS. The authors thank Damon Teagle for comments on an early draft of this manuscript and Edward Gasson for sharing his data for Fig. 3. This work contributes to Natural Environment Research Council (London) (NERC) Grants NE/D00876X/2 and NE/I005596/1 (to G.L.F.), NERC consortium iGlass Grant NE/I009906/1 (to E.J.R.), and 2012 Australian Laureate Fellowship FL120100050 (to E.J.R.). The authors also acknowledge a Royal Society Wolfson Research Merit Award (to E.J.R.).

EARTH, ATMOSPHERIC, AND PLANETARY SCIENCES

1. Meehl GA, et al. (2012) Relative outcomes of climate change mitigation related to global temperature versus sea-level rise. *Nature Climate Change* 2:576–580.
2. Rignot E, Velicogna I, van de Broeke MR, Monaghan A, Lenaerts JTM (2011) Acceleration of the contribution of the Greenland and Antarctic ice sheets to sea level rise. *Geophys Res Lett* 38(L05503), 10.1029/2011GL046583.
3. Rohling EJ, Medina-Elizalde M, Sheppard JG, Siddall M, Stanford JD (2012) Sea surface and high-latitude temperature sensitivity to radiative forcing of climate over several glacial cycles. *J Clim* 25:1635–1656.
4. Rohling EJ, Sluijs A, Dijkstra HA, Köhler P; Paleosens Project Members. Making sense of palaeoclimate sensitivity. *Nature* 491:683–691.
5. Solomon SD, et al., eds (2007) *Contribution of Working Group 1 to the Fourth Assessment Report of the Intergovernmental Panel on Climate Change; The Physical Science Basis* (Cambridge Univ Press, Cambridge, UK), p 996.
6. Petit JR, et al. (1999) Climate and atmospheric history of the past 420,000 years from the Vostok ice core, Antarctica. *Nature* 399:429–436.
7. Siegenthaler U, et al. (2005) Stable carbon cycle-climate relationship during the Late Pleistocene. *Science* 310(5752):1313–1317.
8. Lüthi D, et al. (2008) High-resolution carbon dioxide concentration record 650,000-800,000 years before present. *Nature* 453(7193):379–382.
9. Rohling EJ, et al. (2009) Antarctic temperature and global sea level closely coupled over the past five glacial cycles. *Nat Geosci* 2:500–504.
10. Myhre G, Highwood EJ, Shine KP, Stordal F (1998) New estimates of radiative forcing due to well mixed greenhouse gases. *Geophys Res Lett* 25(4):2715–2718.
11. Peltier WR (2004) Global glacial isostasy and the surface of the ice-age Earth: The ICE-5G (VM2) Model and GRACE. *Annu Rev Earth Planet Sci* 32:111–149.
12. Alley RB, Clark PU, Huybrechts P, Joughin I (2005) Ice-sheet and sea-level changes. *Science* 310(5747):456–460.
13. Pagani M, et al. (2011) The role of carbon dioxide during the onset of Antarctic glaciation. *Science* 334(6060):1261–1264.
14. Sanyal A, et al. (1996) Oceanic pH control on the boron isotopic composition of foraminifera: Evidence from culture experiments. *Paleoceanography* 11(5):513–517.
15. Pearson PN, Foster GL, Wade BS (2009) Atmospheric carbon dioxide through the Eocene-Oligocene climate transition. *Nature* 461(7267):1110–1113.
16. Seki O, et al. (2010) Alkenone and boron based Plio-Pleistocene pCO2 records. *Earth Planet Sci Lett* 292:201–211.
17. Bartoli G, Hönisch B, Zeebe R (2011) Atmospheric CO_2 decline during the Pliocene intensification of Northern Hemisphere glaciations. *Paleoceanography* 26:PA4213, 10.1029/2010PA002055.
18. Foster GL, Lear CH, Rae JWB (2012) The evolution of pCO_2, ice volume and climate during the middle Miocene. *Earth Planet Sci Lett* 341-344:243–254.
19. Jasper JP, Hayes JM (1990) A carbon isotope record of CO_2 levels during the late Quaternary. *Nature* 347(6292):462–464.
20. Sanyal A, Hemming NG, Hanson GN, Broecker WS (1995) Evidence for a higher pH in the glacial ocean from boron isotopes in foraminifera. *Nature* 373:234–236.
21. Hönisch B, Hemming NG (2005) Surface ocean pH response to variations in pCO_2 through two full glacial cycles. *Earth Planet Sci Lett* 236(1-2):305–314.

22. Foster GL (2008) Seawater pH, pCO_2 and $[CO_3^{2-}]$ variations in the Caribbean Sea over the last 130 kyr: A boron isotope and B/Ca study of planktic foraminifera. *Earth Planet Sci Lett* 271:254–266.
23. Beerling DJ, Royer DL (2011) Convergent Cenozoic CO_2 history. *Nat Geosci* 4:418–420.
24. Siddall M, et al. (2003) Sea-level fluctuations during the last glacial cycle. *Nature* 423(6942):853–858.
25. Siddall M, et al. (2004) Understanding the Red Sea response to sea level. *Earth Planet Sci Lett* 225:421–434.
26. Miller KG, et al. (2012) High tide of the warm Pliocene: Implications of global sea level for Antarctic deglaciation. *Geology* 40(5):407–410.
27. Cramer BS, Miller KG, Barrett PJ, Wright JD (2011) Late Cretaceous-Neogene trends in deep ocean temperature and continental ice volume: Reconciling records of benthic foraminiferal geochemistry (delta O-18 and Mg/Ca) with sea level history. *J Geophys Res* 116(C12):C12023, 10.1029/2011JC007255.
28. Kominz MA, et al. (2008) Late Cretaceous to Miocene sea-level estimates from the New Jersey and Delaware coastal plain coreholes: An error analysis. *Basin Res* 20: 211–226.
29. John CM, et al. (2011) Timing and magnitude of Miocene eustacy derived from the mixed siliciclastic-carbonate stratigraphic record of the northeastern Australian margin. *Earth Planet Sci Lett* 304:455–467.
30. Zachos JC, Dickens GR, Zeebe RE (2008) An early Cenozoic perspective on greenhouse warming and carbon-cycle dynamics. *Nature* 451(7176):279–283.
31. Raymo ME, Mitrovica JX, O'Leary MJ, DeConto RM, Hearty PJ (2011) Departures from eustacy in Pliocene sea-level records. *Nat Geosci* 4:328–332.
32. Passchier S, et al. (2011) Early and middle Miocene Antarctic glacial history from the sedimentary facies distribution in the AND-2A drill hole, Ross Sea, Antarctica. *Geol Soc Am Bull* 123(11-12):2352–2365.
33. DeConto RM, Pollard D (2003) Rapid Cenozoic glaciation of Antarctica induced by declining atmospheric CO2. *Nature* 421(6920):245–249.
34. Pollard D, DeConto RM (2009) Modelling West Antarctic ice sheet growth and collapse through the past five million years. *Nature* 458(7236):329–332.
35. Naish T, et al. (2009) Obliquity-paced Pliocene West Antarctic ice sheet oscillations. *Nature* 458(7236):322–328.
36. Tzedakis PC, Channell JET, Hodell DA, Kleiven HF, Skinner LC (2012) Determining the natural length of the current interglacial. *Nat Geosci* 5(2):138–141.
37. Pollard D, DeConto RM (2005) Hysteresis in Cenozoic Antarctic ice-sheet variations. *Global Planet Change* 45:9–21.
38. De Boer B, Van de Wal RSW, Bintanja R, Lourens LJ, Tuenter E (2010) Cenozoic global ice-volume and temperature simulations with 1-D ice-sheet models forced by benthic $\delta^{18}O$ records. *Ann Glaciol* 51(55):23–33.
39. van de Wal RSW, de Boer B, Lourens LJ, Kohler P, Bintanja R (2011) Reconstruction of a continuous high-resolution CO2 record over the past 20 million years. *Clim Past* 7(4): 1459–1469.
40. Gasson E, et al. (2012) Exploring uncertainties in the relationship between temperature, ice volume, and sea level over the past 50 million years. *Rev Geophys* 50: RG1005, 10.1029/2011RG000358.
41. Pfeffer WT, Harper JT, O'Neel S (2008) Kinematic constraints on glacier contributions to 21st-century sea-level rise. *Science* 321(5894):1340–1343.
42. Rohling EJ, et al. (2008) High rates of sea-level rise during the last interglacial period. *Nat Geosci* 1:38–42.
43. Grant KM, et al. (2012) Rapid coupling between ice volume and polar temperature over the past 150,000 years. *Nature* 491(7426):744–747.
44. Archer D, et al. (2009) Atmospheric lifetime of fossil fuel carbon dioxide. *Annu Rev Earth Planet Sci* 37:117–134.
45. Lear CH, Mawbey EM, Rosenthal Y (2010) Cenozoic benthic foraminiferal Mg/Ca and Li/Ca records: Toward unlocking temperatures and saturation states. *Paleoceanography* 25(PA4215), 10.1029/2009PA001880.
46. Hansen JE, Sato M (2012) Paleoclimate implications for human-made climate change. *Climate Change: Inferences from Paleoclimate and Regional Aspects*, eds Berger A, Mesinger F, Šijački D (Springer, Heidelberg), pp 21–48.

Supporting Information

Foster and Rohling 10.1073/pnas.1216073110

SI CO_2 and Sea-Level Estimates

Here, we detail the methodologies used to generate absolute sea-level and atmospheric CO_2 data for each of our studied time periods. All the data used to construct the relationship between CO_2 and sea level described in the main manuscript are listed in Dataset S1, with the exception of the 0–550-kya data, which may be found in ref. 1. The statistical B-spline assessment through these data is summarized in Dataset S2.

Pleistocene (<550 kya). Sea-level estimates for the past 550,000 y come directly from ref. 1, as determined from oxygen isotope ratios of Red Sea foraminifera and bulk sediment (2, 3). Uncertainties in these estimates are ±13 m (at 95% confidence) (1). There is good agreement between these sea-level estimates and independent estimates from coral and speleothem-based sea-level markers (1).

Estimates of atmospheric CO_2 during this period come from measurements of ancient air trapped in ice cores (4–6). These are the highest-fidelity records of atmospheric CO_2 available, and CO_2 records from multiple ice cores drilled covering the last 1000 y agree well but do exhibit small differences (0–6 ppm; 0–2%) (7). We therefore apply a conservative uncertainty of ±10 ppm (at 95% confidence) to these data.

Pliocene (2.7–3.1 Ma). In a recent compilation of sea-level highstands during the Pliocene, sea-level estimates from geochemical (based on the $\delta^{18}O$ of seawater; $\delta^{18}O_{sw}$) and sequence stratigraphic methods were combined (8). The $\delta^{18}O_{sw}$ was determined by several methods: (*i*) scaled from benthic foraminiferal $\delta^{18}O$ (with an assumption regarding the respective importance of ice volume and temperature); and (*ii*) from the $\delta^{18}O$ of benthic foraminifera corrected for temperature using Mg/Ca of benthic foraminifera (9) and ostracods (10). By making assumptions regarding the isotopic composition of the continental ice, an ice-volume calibration (in this case, 0.1‰ per 10 m) may be used to calculate relative sea level. Errors for these estimates relate to uncertainty in temperature and the $\delta^{18}O$ of benthic foraminifera (8). The errors amount to approximately ±13 m (at 95% confidence). Sequence stratigraphic estimates for the Pliocene highstands, as summarized in ref. 8, include (*i*) backstripping of the Eyreville, Virginia, borehole in the moat of the Late Eocene Chesapeake Bay impact structure; (*ii*) backstripping of Wanganui Basin, New Zealand, sediments; and (*iii*) seismic, lithostratigraphic, and chemostratigraphic study of Enewetak Atoll, central Pacific. Uncertainties are around ±10–15 m in methods *i* and *ii*, and ±20 m for *iii*, at 95% confidence (8).

These highstand estimates were combined, and an average and uncertainty were generated; at 95% confidence, these uncertainties ranged from ±7.4 to ±9.8 m (8) (2 se = 2 standard deviation/$\sqrt{n-1}$; where n = number of observations).

Because each highstand has an age uncertainty of ±10,000 y (8), we have combined these averaged Pliocene highstand sea-level estimates with CO_2 estimates from the boron isotopic composition of planktic foraminifera ($\delta^{11}B$) that fall within this age range (11, 12). From $\delta^{11}B$, surface water pH can be estimated and, provided some estimate of a second carbonate system parameter exists, $[CO_2]_{aq}$ and hence atmospheric CO_2 can be calculated (using Henry's law and assuming air–sea equilibrium; see details in refs. 11 and 12). Uncertainty in CO_2 calculated from $\delta^{11}B$ is driven largely by the measurement uncertainty, and the other required variables do not have much impact (11–13). The influence of changing $\delta^{11}B$ of seawater on the CO_2 reconstructions, combined with uncertainties that reflect the influence of other contributing factors, ranges from $^{+66}/_{-56}$ to $^{+107}/_{-89}$ ppm at 95% confidence (12). Seki et al. (11) did not explore the entire range of contributing factors. Therefore, here we have increased the uncertainty for data from that study to ±50 ppm (from ±25 ppm).

Several other methods have been used to estimate CO_2 during the Pliocene [e.g., B/Ca (14), $\delta^{13}C$ of alkenones (15), $\delta^{13}C$ of bulk organic carbon (16), stomatal index of fossil leaves (17); and $\delta^{11}B$ (18)]. However, several techniques used to reconstruct CO_2 in the Pliocene have since been shown to be problematic. For instance, some estimates now are thought to be inaccurate because of issues with the analytical technique (e.g., the $\delta^{11}B$-based record of ref. 18; see discussion in ref. 11) or because the methodology used is either out of date (16) or has since been shown to be more complicated than originally thought (e.g., the B/Ca proxy used by ref. 14; see ref. 19). As highlighted by a recent compilation (20), however, there is a relatively good agreement between the various remaining techniques for this time period (Fig. S1).

Miocene (11–17 Ma). The sea-level data for the Miocene used here are generated using a published record of $\delta^{18}O_{sw}$ (21). This record was produced by correcting the $\delta^{18}O$ of benthic foraminifera from Ocean Drilling Program (ODP) Site 761 for temperature based on Mg/Ca. This approach suffers from the drawback that Mg/Ca in benthic foraminifera also is influenced by $\Delta CO_3^{=}$ (21). Lear et al. (21) attempt to account for this using tandem measurements of Li/Ca in benthic foraminifera [a proxy for deep-water $\Delta CO_3^{=}$ (22)]. We convert this record of $\delta^{18}O_{sw}$ into a record of relative sea-level changes using an ice-volume:sea-level calibration of 0.09–0.11‰ per 10 m, based on a Miocene ice-sheet modeling study (23). It is possible to generate a relative record of sea-level changes using these data only because the Mg/Ca ratio of seawater during the Miocene is poorly known [see Lear et al. (21) and Cramer et al. (41) for further discussion]. This floating sea-level record was then fixed in absolute sea-level space by assuming that the lightest $\delta^{18}O_{sw}$ at 14.8 Ma in the ODP 761 record (21) is temporally coincident with the Miocene highstand (26 ± 18 m) at 14.2 ± 0.5 Ma from the New Jersey margin (NJM) record (24). The latter sea-level record is based on backstripping of marginal sediments from New Jersey combined with estimates of paleo-water depth using detailed lithofacies, ichnological, and benthic foraminiferal analyses (24). Eustatic sea-level changes recorded by the NJM are thought to underestimate changes in actual water depth [termed apparent sea-level changes (25) because of a difference in reference frames (e.g., water depth concerns sea surface to ocean floor whereas the eustasy reference frame is fixed relative to the center of the Earth; see discussion in ref. 25)]. To account for this, following ref. 21 the Miocene highstand estimate is multiplied by 1.48 to convert it to an apparent sea level (25). Uncertainty in our Miocene sea-level record is on average ±21 m (at 95% confidence), which is the root mean square sum of the uncertainty in $\delta^{18}O_{sw}$ (reflecting the range of $\delta^{18}O_{sw}$ from $\Delta CO_3^{=}$ corrected Mg/Ca and uncorrected Mg/Ca), the uncertainty in the NJM highstand (±18 m), and the uncertainty in the ice-volume:sea-level calibration (from 0.09 to 0.11‰ per 10 m). Fig. S2 compares our Miocene sea-level record with the NJM record (24). Clearly there is some discrepancy in terms of absolute magnitude and the timing of sea-level change (but note that the age uncertainty on the NJM record is ±0.5 Ma). It also has been noted that the Miocene is a particularly problematic period for the NJM (26) and similar reconstructions from other locations [e.g., Marion Plateau, Australia (26)] exhibit much greater changes (Fig. S2). The amplitudes of change in the more recent Marion Platform record (26) agree well with our Miocene sea-level record, particularly when the age uncertainty in the former is considered (±0.7 Ma; Fig. S2). It should also be noted that substituting the ODP 761 $\delta^{18}O_{sw}$ with a similar record (27), which made no attempt to correct for the $\Delta CO_3^{=}$ effect on Mg/Ca, yields a sea-level record similar to that shown in Fig. 2.

The CO_2 record we use for the Miocene is based on the $\delta^{11}B$ of planktic foraminifera also recovered from ODP 761, supplemented with samples from ODP 926 (13). Therefore, CO_2 and sea level are reconstructed on exactly the same samples so that there is no uncertainty about the relative timings. The $\delta^{11}B$ proxy is described above, but a complicating factor for the Miocene is the unknown $\delta^{11}B$ of seawater. This value was estimated using several methods, and the uncertainty in this variable does not shift the calculated CO_2 beyond the propagated uncertainties relating to temperature, $\delta^{11}B$ measurements, and uncertainty in the second carbonate system parameter (in this case, total alkalinity) (13). Typical uncertainty in these boron-based atmospheric CO_2 estimates ranges from 36 to 92 ppm, with an average of $^{+55}/_{-53}$ ppm (at 95% confidence).

Once again, several other records of atmospheric CO_2 for this time period are available [e.g., B/Ca (14), $\delta^{11}B$ (18), $\delta^{13}C$ alkenones (28), and stomatal index (29)]. However, the accuracy of the B/Ca-based record (14) and the early $\delta^{11}B$ record (18) are compromised (see above). The $\delta^{11}B$-based record used here agrees well with the stomatal index record (29), but age uncertainties in their terrestrial record preclude it from being combined with sea-level records (Fig. S1). There also is some agreement between the alkenone $\delta^{13}C$ record (28) and the $\delta^{11}B$-based record we use either side of the middle Miocene Climatic Optimum [MCO; 15–16 Ma (13)], however, during the MCO, the alkenone $\delta^{13}C$ record yields CO_2 values that are lower than those from $\delta^{11}B$, which probably relates to the temperature estimates used (28), which are biased to too-low values by diagenesis and incorrect assumptions regarding ice volume (see discussion in ref. 13).

Eocene–Oligocene Boundary (33–35 Ma). Similar to the Miocene, the sea-level data used here for the Eocene–Oligocene boundary are estimated from a reconstruction of $\delta^{18}O_{sw}$ based on the $\delta^{18}O$ of the planktic foraminifer *Turborotalia ampliapertura* (30), corrected for temperature using Mg/Ca data (31). For this approach, we assume that salinity change does not have a large influence on this record (30). We use an ice-volume:sea-level calibration of 0.08–0.15‰ per 10 m to get a relative sea-level record for this time period. We use a larger range here because, unlike the Miocene, no study has directly investigated the likely ice-volume:sea-level calibration for the Eocene–Oligocene; 0.08–0.15‰ per 10 m also encompasses and exceeds the range (0.08–0.12‰ per 10 m) for the last 36 Ma as estimated from ice-sheet modeling and an inversion of the benthic $\delta^{18}O$ record (32, 33). Again, because of a poorly constrained Mg/Ca ratio of seawater during the Late Eocene, it is possible to generate only a relative record of sea level during this interval using this approach. We turn this relative record into an absolute sea-level record by assuming that the lightest $\delta^{18}O_{sw}$ reconstructed = 64 m, which is considered to be sea level in an ice-free world [which the Late Eocene is assumed to approximate (34)]. Uncertainty in this sea-level record (approximately ± 22 to ±40 m at 95% confidence) is a root-mean-square sum of the uncertainty in the $\delta^{18}O_{sw}$ reconstruction (±0.2‰ = ±22 m) and the uncertainty in sea level caused by changing the ice-volume:sea-level calibration from 0.08‰ to 0.15‰ per 10 m (approximately ±1 to ±36 m depending on sea level). Several alternative sea-level records exist for this time period that overlap very well with the record we generate here (Fig. S2).

The CO_2 record we use for the Eocene–Oligocene boundary is the $\delta^{11}B$-based record using the planktic foraminifer *T. ampliapertura* (31). This is by far the highest-resolution record available and uses the same samples used for the sea-level record discussed above. Although questions remain concerning the $\delta^{11}B$ of seawater during this time period and the potential for vital effects in *T. ampliapertura*, in terms of absolute CO_2 this record agrees well with the published alkenone $\delta^{13}C$-based record (35), although the CO_2 estimate from $\delta^{11}B$ consistently is slightly higher (but within uncertainty). Our confidence in our Eocene–Oligocene boundary CO_2:sea-level reconstruction is increased given the good agreement with the longer-term reconstruction for the Eocene and Oligocene discussed below (e.g., Fig. 3).

This Eocene–Oligocene boundary dataset also provides some limited insight into the hysteresis exhibited by the Antarctic Ice Sheet that grew during this time (36). For Fig. 3, we plot only the data in which CO_2 is on a declining trend. At 33.3 Ma, the $\delta^{11}B$-based CO_2 record exhibits a rebound to pre-Eocene–Oligocene boundary CO_2 values (Fig. 2*B*). Although this may be a local signal or an analytical artifact, several other records exhibit at least a partial return to Eocene-like values at roughly this time [e.g., sea-surface temperature records from marginal (30, 37, 38) and deep-ocean sites (39, 40)]. If we assume it is a real signal, then given the general lack of a significant sea-level response at this time, it implies (as suggested by ref. 31) a strong hysteresis for the Eocene–Oligocene Antarctic ice sheet (Fig. S3); i.e., it seems to have been able to survive despite CO_2 rising to ~1,200 ppm for 200,000 y. However, given the limited nature of this dataset, this picture no doubt will be refined further with future studies.

Eocene–Oligocene (20–40 Ma). Sea-level estimates for this time period come from the recent compilation of ref. 41. Here, sea level is extracted from a smoothed and resampled NJM sea-level record capped at 64 m (ice-free Earth; see ref. 41 for full details). The sea-level record produced is available at a temporal resolution of 100,000 y and therefore is readily combined with the CO_2 data generated using the $\delta^{13}C$ alkenone proxy from the same time period (35). We assume a conservative uncertainty in this smoothed sea-level record of ±20 m (at 95% confidence). For simplicity, for the CO_2 record we use only the data from site 925A calculated with TEX_{86} temperatures (see ref. 35 for details). CO_2 values calculated with alkenone temperatures do not differ significantly from these estimates (35). In ref. 35, the authors explore the influence of several key variables on the generated CO_2 record, and here we take the uncertainty at 95% confidence to be the range in CO_2 caused by changing these variables. This treatment results in uncertainties in CO_2 of between 12% and 25%. This CO_2 record agrees well with the relatively poorly dated estimates based on stomatal density in fossil leaves (29, 42, 43) (Fig. S1).

1. Rohling EJ, et al. (2009) Antarctic temperature and global sea level closely coupled over the past five glacial cycles. *Nat Geosci* 2:500–504.
2. Siddall M, et al. (2003) Sea-level fluctuations during the last glacial cycle. *Nature* 423 (6942):853–858.
3. Siddall M, et al. (2004) Understanding the Red Sea response to sea level. *Earth Planet Sci Lett* 225:421–434.
4. Petit JR, et al. (1999) Climate and atmospheric history of the past 420,000 years from the Vostok ice core, Antarctica. *Nature* 399:429–436.
5. Siegenthaler U, et al. (2005) Stable carbon cycle-climate relationship during the Late Pleistocene. *Science* 310(5752):1313–1317.
6. Lüthi D, et al. (2008) High-resolution carbon dioxide concentration record 650,000-800,000 years before present. *Nature* 453(7193):379–382.
7. Ahn J, et al. (2012) Atmospheric CO_2 over the last 1000 years: A high-resolution record from the West Antarctic Ice Sheet (WAIS) Divide ice core. *Global Biogeochem Cycles* 26(GB2027), 10.1029/2012GL053018.
8. Miller KG, et al. (2012) High tide of the warm Pliocene: Implications of global sea level for Antarctic deglaciation. *Geology* 40(5):407–410.
9. Sosdian S, Rosenthal Y (2009) Deep-sea temperature and ice volume changes across the Pliocene-Pleistocene climate transitions. *Science* 325(5938):306–310.
10. Dwyer GS, Chandler MA (2009) Mid-Pliocene sea level and continental ice volume based on coupled benthic Mg/Ca palaeotemperatures and oxygen isotopes. *Philos Transact A Math Phys Eng Sci* 367(1886):157–168.
11. Seki O, et al. (2010) Alkenone and boron based Plio-Pleistocene pCO_2 records. *Earth Planet Sci Lett* 292:201–211.

12. Bartoli G, Hönisch B, Zeebe R (2011) Atmospheric CO_2 decline during the Pliocene intensification of Northern Hemisphere glaciations. *Paleoceanography* 26:PA4213, 10.1029/2010PA002055.
13. Foster GL, Lear CH, Rae JWB (2012) The evolution of pCO_2, ice volume and climate during the middle Miocene. *Earth Planet Sci Lett* 341-344:243–254.
14. Tripati AK, Roberts CD, Eagle RA (2009) Coupling of CO_2 and ice sheet stability over major climate transitions of the last 20 million years. *Science* 326(5958):1394–1397.
15. Pagani M, Liu Z, LaRiviere J, Ravelo AC (2010) High Earth-system climate sensitivity determined from Pliocene carbon dioxide concentrations. *Nat Geosci* 3:27–30.
16. Raymo ME, Grant B, Horowitz M, Rau GH (1996) Mid-Pliocene warmth: Stronger greenhouse and stronger conveyor. *Mar Micropaleontol* 27:313–326.
17. Kürschner WM, van der Burgh J, Visscher H, Dilcher DL (1996) Oak leaves as biosensors of late Neogene and early Pleistocene paleoatmospheric CO_2 concentrations. *Mar Micropaleontol* 27:299–312.
18. Pearson PN, Palmer MR (2000) Atmospheric carbon dioxide concentrations over the past 60 million years. *Nature* 406(6797):695–699.
19. Allen KA, Honisch B (2012) The planktic foraminiferal B/Ca proxy for seawater carbonate chemistry: A critical evaluation. *Earth Planet Sci Lett* 345-348:203–211.
20. Beerling DJ, Royer DL (2011) Convergent Cenozoic CO_2 history. *Nat Geosci* 4:418–420.
21. Lear CH, Mawbey EM, Rosenthal Y (2010) Cenozoic benthic foraminiferal Mg/Ca and Li/Ca records: Toward unlocking temperatures and saturation states. *Paleoceanography* 25(PA4215), 10.1029/2009PA001880.
22. Lear CH, Rosenthal Y (2006) Benthic foraminiferal Li/Ca: Insights into Cenozoic seawater carbonate saturation state. *Geology* 34(11):985–988.
23. Langebroek PM, Paul A, Schulz M (2010) Simulating the sea level imprint on marine oxygen isotope records during the middle Miocene using an ice sheet–climate model. *Paleoceanography* 25(PA4203), 10.1029/2008PA001704.
24. Kominz MA, et al. (2008) Late Cretaceous to Miocene sea-level estimates from the New Jersey and Delaware coastal plain coreholes: An error analysis. *Basin Res* 20:211–226.
25. Pekar SF, Christie-Blick N, Kominz M, Miller KG (2002) Calibration between eustatic estimates from backstripping and oxygen isotopic records for the Oligocene. *Geology* 30:903–906.
26. John CM, et al. (2011) Timing and magnitude of Miocene eustacy derived from the mixed siliciclastic-carbonate startigraphic record of the northeastern Australian margin. *Earth Planet Sci Lett* 304:455–467.
27. Shevenell AE, Kennett JP, Lea DW (2008) Middle Miocene ice sheet dynamics, deep-sea temperatures, and carbon cycling: A Southern Ocean perspective. *Geochem Geophys Geosyst* 9(Q02006), 10.01029/02007GC001736.
28. Pagani M, Freeman KH, Arthur MA (1999) Late miocene atmospheric $CO_{(2)}$ concentrations and the expansion of $C_{(4)}$ grasses. *Science* 285(5429):876–879.
29. Kürschner WM, Kvacek Z, Dilcher DL (2008) The impact of Miocene atmospheric carbon dioxide fluctuations on climate and the evolution of terrestrial ecosystems. *Proc Natl Acad Sci USA* 105(2):449–453.
30. Lear CH, Bailey T, Pearson PN, Coxall HK, Rosenthal Y (2008) Cooling and ice growth across the Eocene-Oligocene transistion. *Geology* 36(2):251–254.
31. Pearson PN, Foster GL, Wade BS (2009) Atmospheric carbon dioxide through the Eocene-Oligocene climate transition. *Nature* 461(7267):1110–1113.
32. Zachos JC, Dickens GR, Zeebe RE (2008) An early Cenozoic perspective on greenhouse warming and carbon-cycle dynamics. *Nature* 451(7176):279–283.
33. de Boer B, van de Wal RSW, Lourens LJ, Bintanja R (2012) Transient nature of the Earth's climate and the implications for the interpretation of benthic $\delta^{18}O$ records. *Palaeogeogr Palaeoclimatol Palaeoecol* 335-336:4–11.
34. Alley RB, Clark PU, Huybrechts P, Joughin I (2005) Ice-sheet and sea-level changes. *Science* 310(5747):456–460.
35. Pagani M, et al. (2011) The role of carbon dioxide during the onset of Antarctic glaciation. *Science* 334(6060):1261–1264.
36. Coxall HK, Wilson PA, Pälike H, Lear CH, Backman J (2005) Rapid stepwise onset of Antarctic glaciation and deeper calcite compensation in the Pacific Ocean. *Nature* 433(7021):53–57.
37. Katz ME, et al. (2008) Stepwise transition from the Eocene greenhouse to the Oligocene icehouse. *Nat Geosci* 11:329–334.
38. Wade BS, et al. (2012) Multiproxy record of abrupt sea-surface cooling across the Eocene-Oligocene transition in the Gulf of Mexico. *Geology* 40:159–162.
39. Liu Z, et al. (2009) Global cooling during the eocene-oligocene climate transition. *Science* 323(5918):1187–1190.
40. Bohaty S, Zachos JC, Delaney ML (2012) Foraminiferal Mg/Ca evidence for Southern Ocean cooling across the Eocene-Oligocene transition. *Earth Planet Sci Lett* 317-318: 251–261.
41. Cramer BS, Miller KG, Barrett PJ, Wright JD (2011) Late Cretaceous-Neogene trends in deep ocean temperature and continental ice volume: Reconciling records of benthic foraminiferal geochemistry (delta O-18 and Mg/Ca) with sea level history. *J Geophys Res* 116(C12):C12023, 10.1029/2011JC007255.
42. Retallack GJ (2009) Greenhouse crises of the past 300 million years. *Geological Society of America Bulletin* 121:1441–1455, 10.1130/B25275.1.
43. Doria G, et al. (2011) Declining atmospheric CO_2 during the late middle Eocene climate transition. *Am J Sci* 311:63–75.

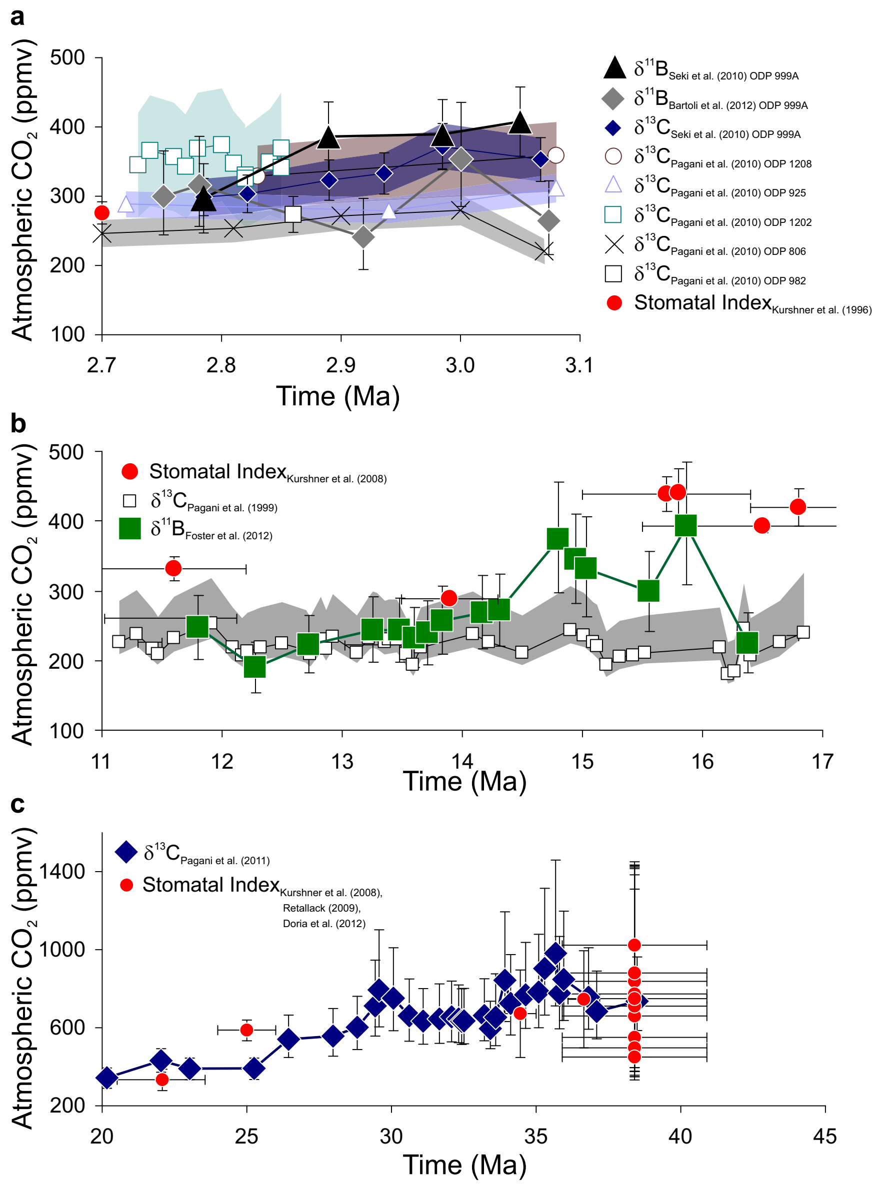

Fig. S1. Comparison of published CO_2 records for the Pliocene (2.7–3.1 Ma), Miocene (11–17 Ma), and Eocene–Oligocene (20–40 Ma). (*A*) $\delta^{11}B$-based CO_2 records used here (11, 12) for the Pliocene (2.7–3.1 Ma) with the multisite $\delta^{13}C$-based estimates of ref. 15 (normalized so that the CO_2 of the youngest sample in the entire record for each site = ice-core CO_2 at that time to remove disequilibrium effects) and the estimate based on stomatal index of fossil leaves (17). (*B*) $\delta^{11}B$-based CO_2 record used here (13) for the Miocene (11–17 Ma) with the $\delta^{13}C$-based record (28) and the stomatal index-based estimates (29). (*C*) $\delta^{13}C$-based record used here for the Eocene–Oligocene (35) with stomatal index-based estimates (29, 42, 43). In all cases, the uncertainty (either error bar or band) is at 95% confidence.

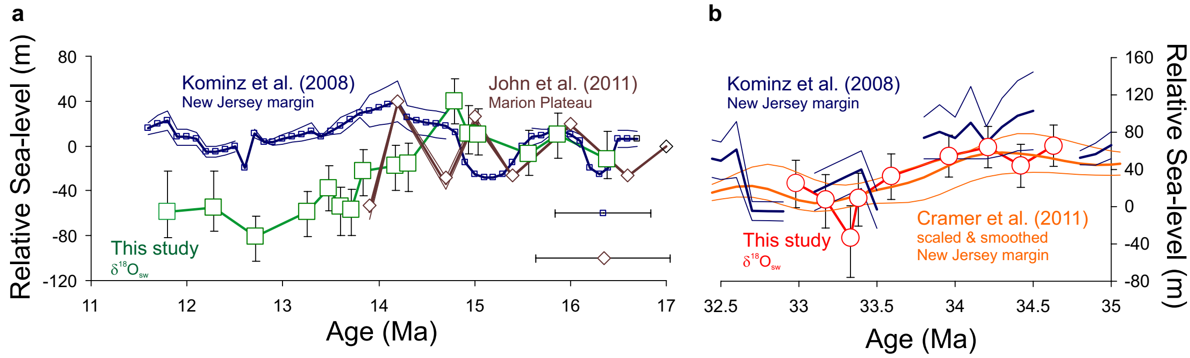

Fig. S2. Comparison of sea-level records for the Miocene (11–17 Ma) and Eocene–Oligocene boundary (32.5–35 Ma). (*A*) Sea-level record used here for the Miocene based on $\delta^{18}O_{sw}$ (green) compared with the records from the NJM (blue) (24) and Marion Plateau (brown) (26) based on backstripping. Note the age uncertainty for the backstripping methods is ±0.7 Ma (Marion Plateau) (26) and ±0.5 Ma (NJM) (24). (*B*) Sea-level record used here for the Eocene–Oligocene based on $\delta^{18}O_{sw}$ (red) compared with the raw (blue) (24) and smoothed and resampled (orange) (41) NJM record. In all cases, the uncertainty (either error bar or band) is at 95% confidence.

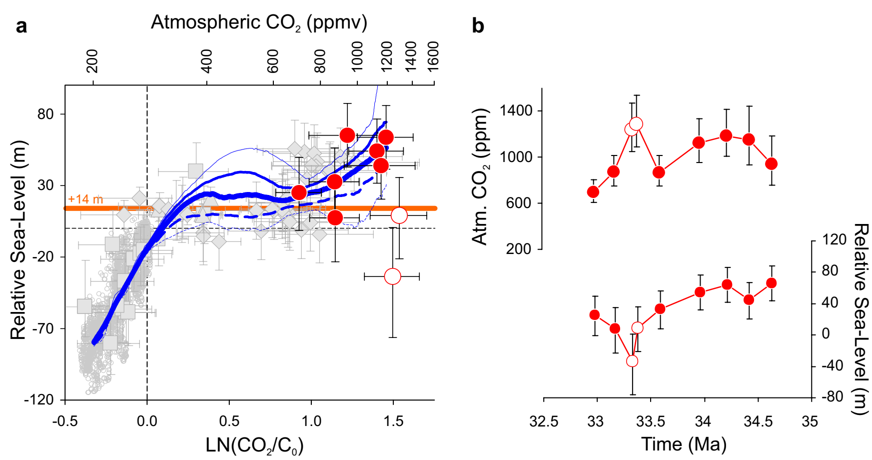

Fig. S3. Possible evidence of hysteresis during the Eocene–Oligocene. (*A*) Fig. 3*C* with all atmospheric CO_2 and sea-level data from the Eocene–Oligocene (Fig. 3*A* shows just the decline in CO_2; closed symbols). All other symbols as in Fig. 3. (*B*) Time series showing all data, with the data from the rebound in CO_2 at ~33.3 Ma highlighted (open symbols).

Other Supporting Information Files

Dataset S1 (XLS)
Dataset S2 (XLS)